# Experimental Investigation of Dispersed Flow Heat Transfer in Curved Tubes

Lautenschlager G., Mayinger F.

Lehrstuhl A für Thermodynamik
Technische Universität München, FRG

## Abstract

When dispersed flow enters a heated bend, heat transfer at the outer side is improved, due mainly to impacting droplets which can even rewet the outer wall, under favourable circumstances. At the inner side of the bend the wall temperatures first increase to a maximum, after an axial distance however, heat transfer is improved too, due to an inward secondary flow bringing coolant from the outer side.

Experiments were carried out with refrigerant R12 in electrically heated circular 90°-bends and in a 450°-coil at different mass flow rates ($400 - 2000\ kg/m^2s$) critical pressure ratios ($0.23 - 0.93$), heat flux densities ($20 - 70\ kW/m^2$), and diameter ratios ($14 - 42$).

For the technically more important case of non-rewetting a model was developed predicting wall temperatures at the outer and inner side of the bend, yielding good agreement with experimental results.

## Nomenclature

| | |
|---|---|
| $w$ | velocity $[m/s]$ |
| $\dot{m}$ | mass flux density $[kg/m^2s]$ |
| $\dot{x}$ | quality [–] |
| D | tube diameter $[m]$ |
| $D_c, R_c$ | diameter, radius of curvature $[m]$ |
| $\dot{q}$ | heat flux density [W] |
| S | slip ratio $(w_v/w_l)$ |
| T | temperature [K] |
| h | enthalpy $[kJ/kg]$ |
| $\dot{M}$ | mass flow rate $[kg/s]$ |
| $\rho$ | density $[kg/m^3]$ |
| $\beta$ | axial distance [degree] |
| $\varphi$ | circumferential distance [degree] |
| $\alpha$ | heat transfer coefficient $[W/m^2K]$ |
| $\lambda$ | thermal conductivity $[W/mK]$ |

Subscripts

| | |
|---|---|
| $v$ | vapour |
| $l$ | liquid |
| $is, os$ | inner,outer side (flow region) |
| $tot$ | total |
| $sat$ | saturation |
| $w$ | wall |
| $d$ | droplet |

## 1. Introduction

In recent years, there has been a large amount of research in the field of dispersed flow heat transfer, motivated by engineering needs in thermohydraulics of nuclear reactor safety. However, most of the experimental work has been carried out in straight, mainly vertical tubes, with little work being done in curved tubes. This may be due to the very complicated fluiddynamic processes occuring in curved flows.

The flow in a curved tube is three-dimensional due to a secondary flow superimposing upon the main flow. The centrifugal force produces a pressure gradient over the cross-section, assuming its maximum value at the outer and the minimum at the inner side of the bend. In the core of the flow, the fluid moves towards the outer side owing to centrifugal force. Close to the wall, where friction prevails, there is an inward flow due to the mentioned pressure difference. By this process the secondary flow forms a pair of vortices, as sketched in fig.1.

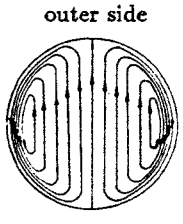


Fig. 1: Streamlines of the secondary flow

Although a considerable number of papers have been published on two phase flow in curved and coiled tubes, there have been comparatively few detailed studies of heat transfer, especially in the post-dryout region. Some investigators reported on two phase flow patterns in coils /1, 2/, but mainly at adiabatic air-water-flow. Most papers on two phase flow heat transfer in curved tubes are confined to conditions where the heated wall is completely wetted /3 – 5/ and correlations only exist for circumferentially averaged heat transfer coefficients. Various investigations were carried out on critical heat flux in curved tubes /6 – 9/. These studies concentrated on the onset of dryout, which occured in the course of the coil. Some of the findings are summarized in /9/.

In contrast to the above mentioned studies the dryout in the experiments carried out occured a long distance before the curved tube. Thus, dispersed flow with thermal nonequilibrium and definite conditions already exist at the bend inlet.

## 2. Experiments

The experiments were carried out with freon R12 in a test-loop, which is shown in fig. 2. The main components of the loop are a centrifugal pump, a preheater, an evaporator, the test section and a condenser. The test section consists of a straight vertical tube and a joint 90°-bend or a 450°-coil, respectively. The tube is made of stainless steel with an inner diameter of 28.5 mm and an outer diameter of 33.7 mm. Differences in the wall thickness resulting from bending the tube range between 1.2 and 4.6% of the wall thickness. The test section is uniformly heated by direct current.

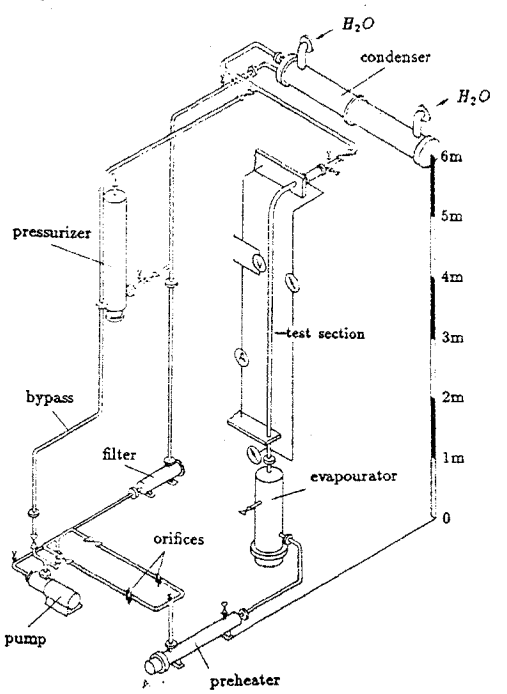


Fig. 2: Test-loop

The wall temperatures are measured by 60 thermocouples (0.5 mm in diameter) which are distributed over the tube length and circumference.
The vapour temperature is measured in two different ways. On one hand bare thermocouples are used, that is to say, the thermocouples are not shielded from impacting droplets. On the other hand a vapour probe is employed which utilizes inertial separation of liquid droplets from vapour. The probe is movable in the cross section, which allows local measurements of the vapour temperature and undisturbed flow during the measurements of the wall temperatures.

Right after the bend outlet a so-called impedance-void-meter is installed for measuring the droplet concentration in different areas of the cross section. It consists of thin concentric tubes wired to 5 separate capacitors which are supplied with a high frequency voltage. The measuring technique bases on the difference between the dielectric constant of liquid and vapour. The measured capacities are used as criterions for different vapour fractions.

A detailed description of experimental apparatus can be found in /10/ and /11/.

Heat transfer measurements were performed in 90°-bends with 200 mm and 610 mm diameters of curvature, respectively, and in a 450°-coil ($D_c = 400mm$) at various parameters listed in the following tabulation:

| | | | |
|---|---|---|---|
| mass flow rate | $\dot{m}\,[kg/m^2s]$ | : | 400, 680, 1240, 2000 |
| heat flux density | $\dot{q}\,[kW/m^2]$ | : | 20, 30, 40, 50, 60, 70 |
| pressure | $p\,[bar]$ | : | 9.5, 19.0, 28.5, 38.0 |
| pressure ratio | $p/p_{crit}$ | : | 0.23, 0.46, 0.70, 0.93 |
| diameter ratio | $D_c/D$ | : | 14, 28, 42 |

Tabulation 1: Experimental matrix

These parameters were restricted by film boiling in the straight test section and wall temperatures over 250°C The quality $\dot{x}$ at the test section inlet was adjusted means of the evaporator in such a way that the dry always occured 2.5 m before the bend inlet yielding t conditions as shown in fig. 3.

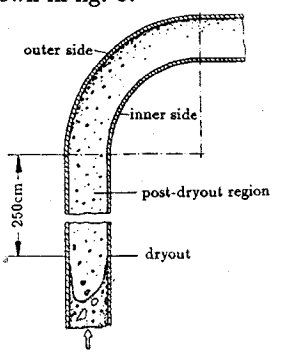


Fig. 3: Dispersed flow in a vertical bend

## 3. Fluid– and Thermodynamic Processes

When dispersed flow enters a curved tube different heat transfer mechanisms take place alonge the circumference, as can be seen from the different wall temperatures at the outer and inner side of the bend, respectively (fig. 4). This difference in heat transfer is mainly due to 3 processes: the change in velocity profile, the outward droplet displacement, and the onset of a secondary flow.

As Ito /12/ found out, the radial pressure gradient induced by the centrifugal force influences the flow several diameters before the bend inlet and over a long distance (30 – 50 D) after the bend outlet. However, this has little effect on heat transfer in our experiments. Downstream, in the bend the velocity maximum shifts towards the outer side, which was confirmed by experimental and numerical investigations /13 – 15/. This process affects heat transfer considerably.

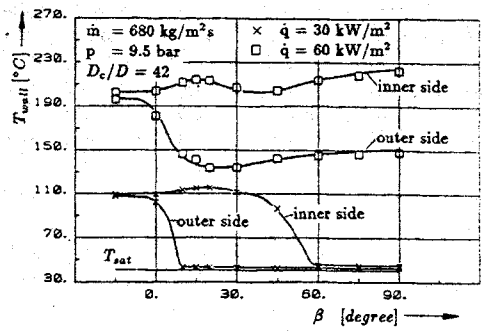


Fig. 4: Wall temperatures at the outer and inner side

However, the main difference between outer and inner side heat transfer is due to the transverse motion of the droplets impinging on the outer wall and improving heat transfer there. Under favourable circumstances even rewetting of the outer wall is possible (fig. 4). In the case that no rewetting occurs, two different regions can be distinguished at the outer side. In the first one, right after the bend inlet, there is a steep decrease in wall temperature due to the impinging droplets (fig. 4). In the following second region, the influence of the droplets upon heat transfer is appreciably reduced and the wall temperatures remain constant or even increase. This is due to the following reason: Large droplets are deflected less by vapour flow than smaller ones. Therefore, at the bend inlet, mainly large droplets with high impact velocity impinge on the outer wall leading to the above mentioned steep temperature drop. Droplets reaching the outer wall in the second region are smaller, with lower impact velocity and do not improve heat transfer considerably.

At the inner side the wall temperatures first increase to a maximum, due to the reduction of flow velocity and the liquid deficiency, and then decrease owing to the secondary flow bringing coolant from the outer side (fig.4). If the outer wall is rewetted, a liquid film can spread along the circumference up to the inner side.

These examples illustrate that heat transfer at the inner side strongly depends on the conditions at the outer side due to secondary flow, and changes in the heat transfer at the outer side can be noticed at the inner side after an axial distance.

## 4. Influence of Experimental Parameters upon Heat Transfer

The influence of parameters varied in the experiments on heat transfer is manifold and cannot be discussed thoroughly here. A detailed study can be found in /11/. In the following only the most important results are briefly explained.

### Influence of reduced pressure ratio

The influence of reduced pressure ratio $p/p_{crit}$ upon heat transfer is shown in fig. 5. As can be seen, the difference between heat transfer in the straight and in the curved tube decreases with a rising pressure ratio, along with the ability of the droplets to rewet the outer wall. These facts are due mainly to the decreasing flow velocity and the increasing density ratio $\rho_v/\rho_l$ which are

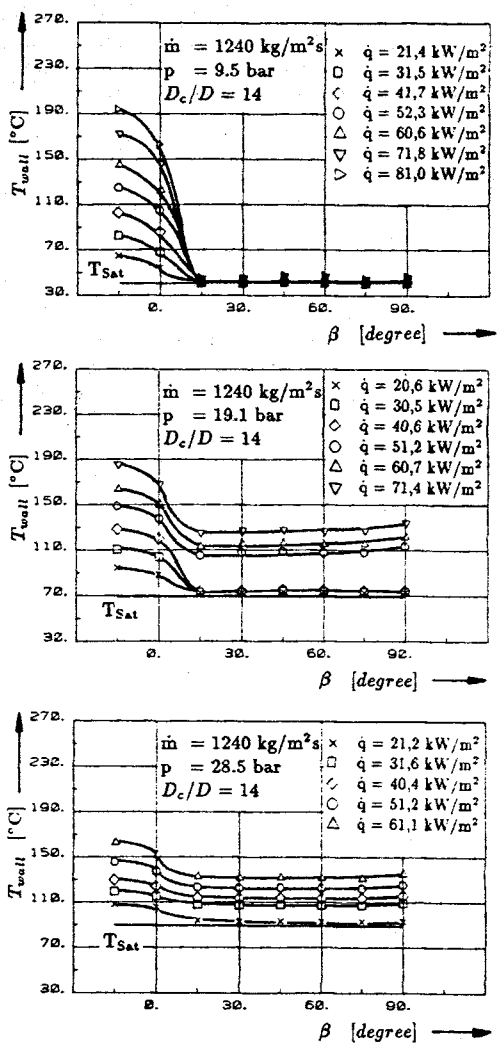


Fig. 5: Influence of pressure ratio upon heat transfer

associated with higher pressure. Thereby the droplets are deflected stronger by vapour flow yielding a smaller number of droplets impacting on the outer wall and lower heat transfer coefficients.

### Influence of mass flow rate

An increase in mass flow rate leads to better heat transfer in the straight and in the curved tube. This is due mainly to higher vapour velocity, which can be explained in heat transfer correlations by a higher Reynolds-number.

If rewetting occurs the circumferential spreading of the liquid film depends on mass flow rate, as can be seen from the wall temperatures at the inner side in fig. 6. The temperature profiles show a maximum, followed by a slight decrease owing to the secondary vapour flow, and then an abrupt drop indicating the onset of rewetting. This sharp change in temperature gradient can be utilized as a criterion of how fast the liquid film spreads along the

circumference. The experimental data show that with rising mass flow rate the onset of rewetting at the inner side shifts towards larger bend angles, meaning, the primary velocity of the liquid film increases faster than the secondary one.

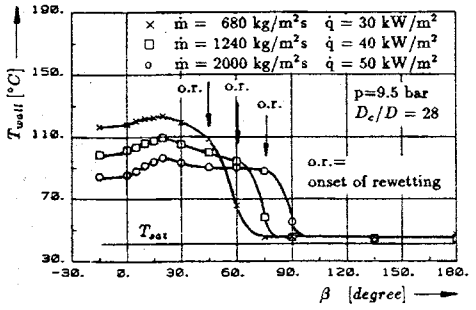


Fig. 6: Influence of mass flow rate upon spreading of the liquid film

## Influence of curvature

Variations of the diameter of curvature mainly affect the circumferential spreading of the liquid film. With rising diameters of curvature the radial pressure gradient and consequently the secondary flow decrease, but the length of the bend increases. The experimental data from fig. 7 shows that with increasing diameter ratio $D_c/D$ the liquid film covers a larger circumferential distance within a definite bend angle $\Delta\beta$. That is to say, the onset of rewetting at the inner side occurs at smaller bend angles $\beta$. In order to maintain clearness of the plot, the temperature profile for the smallest diameter ratio examined ($D_c/D = 14$) is not plotted in fig. 7. In this case, however, the liquid film does not reach the inner side within the 90°-bend.

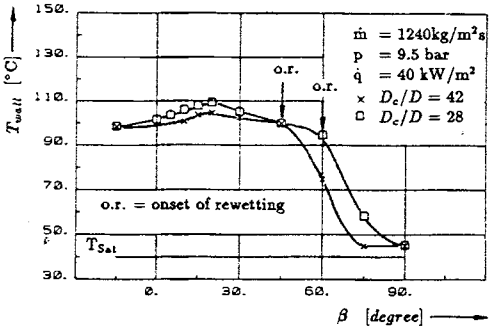


Fig. 7: Influence of curvature

## 5. Distribution of Droplets

Due to the centrifugal force the distribution of droplets becomes inhomogeneous in the course of the bend. Vapour fractions were measured right after the bend outlet in five separate areas of the cross section with the capacitive probe.

Fig.8 displays mean vapour fractions at high mass flow rate and conditions of rewetting. As mentioned previously the velocity of circumferential spreading of the liquid film is low under these conditions. This is confirmed by the data of fig. 8, showing that most of the liquid phase is in the outer region, which rapidly decreases towards the inner side. The high vapour fraction in the core of the flow indicates that most of the droplets have deposited at the outer wall.

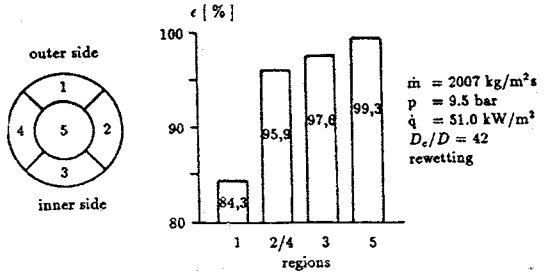


Fig. 8: Vapour fractions at high mass flow rate

Fig. 9 shows mean vapour-fractions characteristic for experiments where rewetting of the wall does not occur. In this case droplet flow is only encountered in the outer side region, that is to say, a circumferential spreading of droplets is not possible. This can be explained as follows: At high wall superheats droplets are pushed out of the thin boundary layer where the inward flow occurs, owing to non-uniform evaporation, before covering a noticeable distance in circumferential direction. Therefore, a measurable amount of liquid can move inward only in the case that rewetting occurs, and then mainly as a thin film.

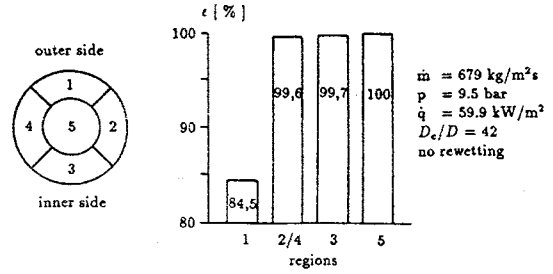


Fig. 9: Vapour fractions in the case of non-rewetting

## 6. Model and Correlations

For the technically more important case of non-rewetting a model was developed predicting wall temperatures at the outer and inner side of the bend. Due to different vapour velocities, vapour temperatures and droplet concentrations at the outer and inner side of the bend, shown in fig. 10, the flow channel is divided in an inner and an outer section. Each is considered separately and flow conditions are defined which are representative for the outer and inner side.

### Vapour Velocity

Dispersed flow is considered very similar to single phase vapour flow. Soo /16/ confirmed that gas velocity profiles in turbulent flow were unchanged with the addition of solid particles (10 to 250 $\mu$m). According to computations by Patankar /14/ and measurements by Rowe

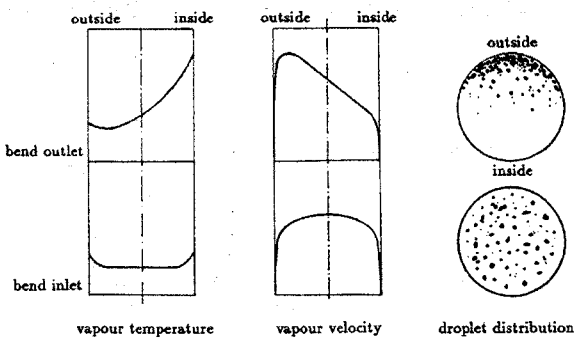


Fig. 10: Flow conditions at the bend inlet and outlet

/13/ the change in velocity profiles is assumed to be small from a distance of 45°. Downstream the flow is considered to be developed with a constant velocity ratio between outer and inner flow region, which can be well approximated – according to measurements by Mori/Nakayama /15/ and Hogg /17/ – by $w_{os}/w_{is} = 2$, in the range of curvature examined. Assuming a slip ratio S=1 the equations for vapour velocity in the inner and outer flow region are:

$$w_{v,is} = \dot{m}_{is} \left( \frac{1-\dot{x}}{\rho_l} + \frac{\dot{x}}{\rho_{v,is}} \right) \quad (1)$$

$$w_{v,os} = \dot{m}_{os} \left( \frac{1-\dot{x}}{\rho_l} + \frac{\dot{x}}{\rho_{v,os}} \right) \quad (2)$$

The continuity equation yields:

$$\dot{m}_{is} + \dot{m}_{os} = 2\, \dot{m}_{tot} \quad (3)$$

The increase and decrease in vapour velocity is approximated by a cosine-function as follows:

$$\begin{aligned} w_{v,is} &= w_m\, K_{(\beta)} \\ w_{v,os} &= w_m\, (2 - K_{(\beta)}) \end{aligned}$$

$$\begin{aligned} K_{(\beta)} &= 0.833 + 0.167\, cos(4\,\beta) \quad \beta < 45° \\ K_{(\beta)} &= 0.666 \qquad\qquad\qquad\qquad \beta \geq 45° \end{aligned} \quad (4)$$

Elimination of the mean velocity $w_m$ results in

$$w_{v,is} = w_{v,os} \frac{K_{(\beta)}}{2 - K_{(\beta)}} \quad . \quad (5)$$

Introducing the relations

$$C_{is} = \frac{1-\dot{x}}{\rho_l} + \frac{\dot{x}}{\rho_{v,is}}, \qquad C_{os} = \frac{1-\dot{x}}{\rho_l} + \frac{\dot{x}}{\rho_{v,os}}$$

the equations of vapour velocities are obtained from equations 1 to 5 as

$$w_{v,is} = \frac{2\, \dot{m}_{tot}\, C_{os}}{\frac{2-K_{(\beta)}}{K_{(\beta)}} + \frac{C_{os}}{C_{is}}} \quad (6)$$

$$w_{v,os} = w_{v,is} \frac{2 - K_{(\beta)}}{K_{(\beta)}} \quad . \quad (7)$$

## Heat Transfer at the Outer Region

Heat transfer at the outer wall of the bend is assumed to consist of two heat transfer paths: from wall to vapour $\dot{q}_{wv,os}$ and from wall to droplets $\dot{q}_{wd}$:

$$\dot{q}_{w,os} = \dot{q}_{wv,os} + \dot{q}_{wd} \quad . \quad (8)$$

Heat transfer contribution of vapour flow is evaluated according to correlations for straight tubes

$$\dot{q}_{wv,os} = \alpha_{wv,os}\, (T_{w,os} - T_{v,os}) \quad (9)$$

applying the Groeneveld-Delorme-equation /18/

$$\alpha_{wv,os} = 0.008348\, \frac{\lambda_{v,os}}{D}\, Re^{0.8774}\, Pr^{0.6112} \quad . \quad (10)$$

The Reynolds-number is calculated with vapour velocity from equation (7).

Heat flux transferred to impacting droplets $\dot{q}_{wd}$ can be calculated from the droplet-mass-transfer rate per surface area $\dot{m}_d$, the effectiveness of individual droplets $\varepsilon$ (= fraction of the droplet which is evaporated on impact with wall), and the heat of evaporation $h_{fg}$:

$$\dot{q}_{wd} = \dot{m}_d\, \varepsilon\, h_{fg} = E\, h_{fg} \quad . \quad (11)$$

As $\dot{m}_d$ and $\varepsilon$ are difficult to determine, the term $E = \dot{m}_d\, \varepsilon$ is correlated by an empirical equation. In axial direction ($\beta$-direction) E rises from zero at the bend inlet ($\beta = 0$) up to a maximum $E_{max}$ at a distance $\beta_{max}$, depending on the liquid mass deposited on the wall, and then decreases due to evaporation and the reduction in droplet supply. The largest E-values occur at the outer surface line decreasing in circumferential direction ($\varphi$-direction) as follows:

$$E_{(\beta,\varphi)} = E_{(\beta,\varphi=0)} \cdot cos\varphi \qquad 0° < \varphi < 90° \quad . \quad (12)$$

The maximum $E_{max}$ at the outer side ($\varphi = 0$) was correlated from the present experimental results as:

$$\frac{E_{max}}{\dot{m}} = a \left( \frac{T_{w,os} - T_{sat}}{T_{sat}} \right)^b \left( \frac{1-\dot{x}}{\dot{x}} \right)^c \left( \frac{D_c}{D} \right)^d \left( \frac{\rho_v}{\rho_l} \right)^e \quad (13)$$

a=1.1 · $10^{-3}$, b=0.774, c=−0.069, d=−0.458, e=0.234. Wall superheats ($T_{w,os} - T_{sat}$), quality $\dot{x}$ and vapour density $\rho_v$ in equation (13) are quantities existing at the bend inlet. The axial distance $\beta_{max}$ where $E_{max}$ occurs resulted from experiments as

$$\begin{aligned} \beta_{max} &= 15° && \dot{x} < 0,70 \\ \beta_{max} &= 34,4 \cdot \left( \frac{D_c}{D} \right)^{-0,32} \left( \frac{1-\dot{x}}{\dot{x}} \right)^{-0,42} && \dot{x} \geq 0,70 \end{aligned} \quad (14)$$

The course of $E_{(\beta)}$ at the outer side ($\varphi = 0$) was approximated by

$$\begin{aligned} E_{(\beta)} &= E_{max} \cdot \left[ 0,5 - 0,5\, cos \left( \frac{\beta\, \pi}{\beta_{max}} \right) \right] && \beta \leq \beta_{max} \\ E_{(\beta)} &= E_{max} \cdot \frac{\beta}{a_o \beta^2 + b_o \beta + c_o} && \beta > \beta_{max} \end{aligned} \quad (15)$$

$a_o = 1/(12 \cdot \beta_{max})$, $b_o = 5/6$, $c_o = \beta_{max}/12$

In order to compute wall temperatures at the outer side the gradients of quality $d\dot{x}/dL$ and of vapour temperature $dT_{v,os}/dL$ are required. The increase in quality in an increment $\Delta L$ only depends on the heat transfered to the droplets $\dot{Q}_{wd}$

$$d\dot{x} = \frac{d\dot{Q}_{wd}}{\dot{M}_{tot}\, h_{fg}} \quad . \tag{16}$$

$$d\dot{Q}_{wd} = E_{(\beta,\varphi=0)} \cdot h_{fg} \cdot D\, dL \quad .$$

The increase in vapour temperature in the outer flow region can be evaluated as:

$$dT_{v,os} = \left( \frac{\dot{q}_w\, \pi\, D\, dL}{2\, \dot{M}_{os}\, \dot{x}} - \frac{d\dot{Q}_{wd}\, (h_{v,os} - h_l)}{\dot{M}_{os}\, h_{fg}\, \dot{x}} \right) \frac{1}{c_{p,v}} . \tag{17}$$

$$\dot{M}_{os} = \frac{\dot{M}_{tot}}{1 + \frac{C_{os}}{C_{is}} \left( \frac{2 - K_{(\beta)}}{K_{(\beta)}} \right)} \quad .$$

## Heat Transfer at the Inner Region

At the inner section of the bend only heat transfer from wall to vapour is considered. Heat flux density is evaluated similar to equation (9), applying the Groeneveld-Delorme-equation (equ.10), however, calculating the Reynolds-number with vapour velocity from equation (6).

$$\dot{q}_{wv,is} = \alpha_{wv,is}\, (T_{w,is} - T_{v,is})\, F \quad . \tag{18}$$

The influence of secondary flow upon heat transfer is taken into consideration by the factor F. F is correlated by an empirical equation from the experimental results as follows:

$$\begin{aligned} F_\beta &= 1 && \beta < 13^\circ \\ F_\beta &= F_{max} \left[ 0{,}5 - 0{,}5\, cos \left( \frac{\beta\, \pi}{46} \right) \right] && 13^\circ < \beta < 46^\circ \\ F_\beta &= F_{max} \left[ \frac{\beta}{a_1 \beta^2 + b_1 \beta + c_1} \right] && \beta \geq 46^\circ \end{aligned} \tag{19}$$

$a_1 = 1.81 \cdot 10^{-3}$, $b_1 = 0.833$, $c_1 = 3.833$.

The maximum $F_{max}$ was correlated as a function of Reynolds-, Prandtl- number, diameter ratio and density ratio existing at the bend inlet as:

$$F_{max} = a\, Re^b\, Pr^c \left( \frac{D_c}{D} \right)^d \left( \frac{\rho_v}{\rho_l} \right)^e \tag{20}$$

$a = 39.2$, $b = -0.333$, $c = -0.345$, $d = -0.071$, $e = -0.085$.

The gradient of vapour temperature in the inner flow region $dT_{v,is}/dL$ can be easily evaluated from equation (17), when the term considering heat transfer from wall to droplets is omitted and the mass flow in the inner region is applied:

$$dT_{v,is} = \frac{dh_{v,is}}{c_{p,v}} = \left( \frac{\dot{q}_w\, \pi\, D\, dL}{2\, \dot{M}_{is}\, \dot{x}} \right) \frac{1}{c_{p,v}} \quad . \tag{21}$$

$$M_{is} = \frac{\dot{M}_{tot}}{1 + \frac{C_{is}}{C_{os}} \left( \frac{K(\beta)}{2 - K(\beta)} \right)}$$

## Comparison of Computation with Experiment

When the flow conditions at the bend inlet are determined by correlations for straight tubes, the wall temperatures at the outer and inner side of the bend can be computed by the equations explained in the preceding section. Figures 11 provides a comparison of predicted wall temperatures and experimental results for 90°-bends, and for the coil up to a distance of 180°. Data from distances larger than 225° could not be analysed, because at this distance the flow was strongly disturbed by a welding seam.

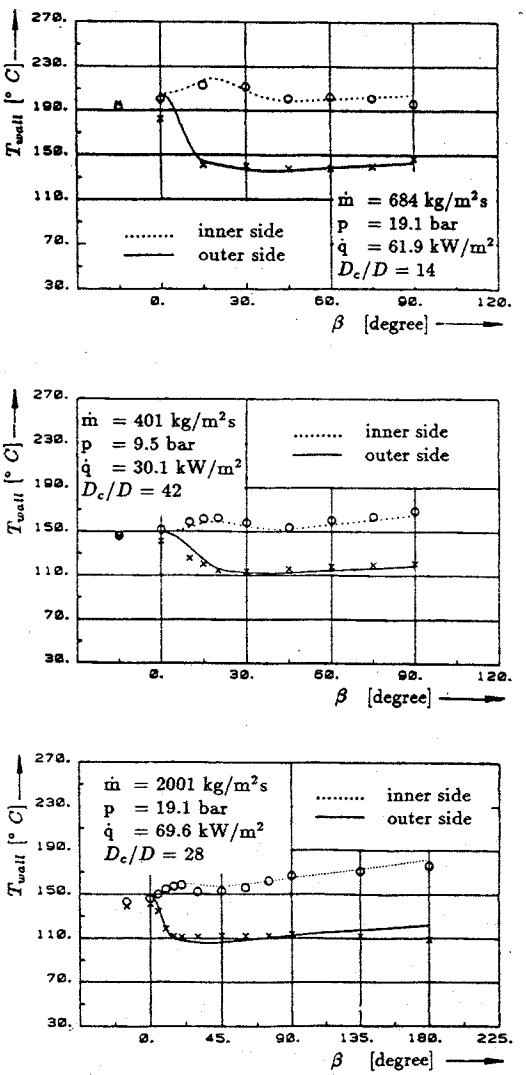


Fig. 11: Comparison of computation with experiment

The model was checked at 47 different flow conditions in the following parameter range:

$\dot{m}$ = 400 bis 2000 $kg/m^2s$
$\dot{q}$ = 30 bis 70 $kW/m^2$
p = 9,5 und 19,1 bar
$D_c/D$ = 14 bis 42
$\beta$ = 0 bis 180° .

yielding good agreement with experimental results.

## 7. Conclusions

In the present study dispersed flow heat transfer in bends was investigated experimentally in a large range of parameters. The most important heat transfer mechanisms and the influence of various flow conditions upon heat transfer were pointed out. A model was developed predicting wall temperatures at the outer and inner side of the bend, for conditions of non-rewetting. There was good agreement between predicted and measured wall temperatures, however, more information about developing flow in bends is required, in order to replace empirical correlations by theoretical equations.

## Acknowledgement

The author wishes to thank the Deutsche Forschungsgemeinschaft (DFG) which supported this work.

## References

/1/ Banerjee S., Rodes E., Scott D.S., Film inversion of cocurrent two-phase flow in helical coils, AICHE J., Vol. 13, No. 1, pp 189 - 191, 1967

/2/ Whalley P.B., Air-water two-phase flow in a helically coiled tube, Int. J. Multiphase Flow, Vol.6, pp 345 - 356, 1980

/3/ Owhadi A., Bell K.J., Crain B., Forced convection boiling inside helically-coiled tubes, Int. J. Heat Mass Transfer, Vol. 11, pp 1779 - 1793, 1968

/4/ Kozeki M., Film thickness and flow boiling in two-phase annular flow in a helically coiled tube, Proc. Intern. Meeting on reactor Heat Transfer, Gesellschaft für Kernforschung, Karlsruhe, 1973

/5/ Chen X., Zhou F., Forced convection boiling and post-dryout heat transfer in helical coiled tube, Proc. Int. Heat Transfer Conf., San Francisco, pp 2221 - 2226, 1986

/6/ Carver J.G., Kakalara C.R., Slotnik J.S., Heat transfer in coiled tubes with two phase flow, Atomic Energy Commision Document, T.I.D. 20938, 1964

/7/ Miropolskiy Z.L., Pikus V.Y., Critical boiling heat fluxes in curved channels, Heat Transfer - Soviet Research, Vol. 1, No 1, 1969

/8/ Cumo M., Farello G.E., Ferrari G., The influence of curvature in post dryout heat transfer, Int. J. Heat Mass Transfer, Vol.15, pp 2045 - 2062, 1972

/9/ Jensen M.K., Bergles A.E., Critical heat flux in helically coiled tubes, J. Heat Transfer, Vol. 103, pp 660 – 666, 1981

/10/ Lautenschlager G., Mayinger F., Post-dryout heat transfer to R12 in circular 90°-tube-bends, Int. Heat Transfer Conference, San Francisco, USA, 1986

/11/ Lautenschlager G., Wärmeübergang in Krümmern bei Sprühkühlung, Dissertation, Technische Universität München, 1988

/12/ Ito H., Pressure losses in smooth pipe bends, Transaction of the ASME, J. of Basic Engineering, pp 131 - 143, March 1960

/13/ Rowe M., Masurements and computations of flow in pipe bends, J. Fluid Mech., Vol. 43, part 4, pp 771 - 783, 1970

/14/ Patankar S.V., Pratap V.S., Spalding D.B., Prediction of turbulent flow in curved pipes, J. Fluid Mech., Vol. 67, part 3, pp 583 - 595, 1975

/15/ Mori Y., Nakayama W., Study on forced convective heat transfer in curved pipes (2nd repord, turbulent region), Int. J. Heat Mass Transfer, Vol. 10, pp 57 - 59, 1967

/16/ Soo S.L., Trezek G.J., Dimick R.C., Hohnstreiter G.F, Concentration and mass flow distribution in a gas-solid suspension, Industrial and Engineering Chemistry Fundamentals, 3, pp 98 - 106, 1964

/17/ Hogg G.W., Ph. D. thesis, University of Idaho, 1968

/18/ Groeneveld D.C., Delorme G.G.J., Prediction of thermal non-equilibrium in the post-dryout regime, Nuclear Engineering and Design 36, pp 17 - 26, 1976